Wave interference effects on two advancing ships

Zhi-Ming Yuan

Dep. of Naval Architecture, Ocean & Marine Engineering, University of Strathclyde, Henry Dyer Building, G4 0LZ, Glasgow, UK

Zhiming.yuan@strath.ac.uk

Highlights

- Development of a method to predict the critical line between the quiescent and wake region.
- Validation of the theoretical estimation based on large amount of numerical calculations.
- Calculation of how much in percentage the wave interference effects are predicted.

Introduction

For a single marine vessel advancing in calm-water, the so-called Kelvin wake can be observed. It is set up by a ship in steady motion and to be confined within a wedge of semi-angle sin-1(1/3) in deep water, which indicates that the free surface can be divided into two regions by a critical line: wake region confined within the Kelvin angle and quiescent region outside the Kelvin angle. For the ships travelling in waves, except the Kelvin wave system, there exist two ($\tau > 0.25$, $\tau = \omega_e u_0 / g$, ω_e is the encounter frequency, u_0 is the forward speed, and g is the gravity acceleration) or three ($\tau < 0.25$) unsteady wave systems due to the oscillation of the ship (Becker, 1958; Wehausen, 1960).

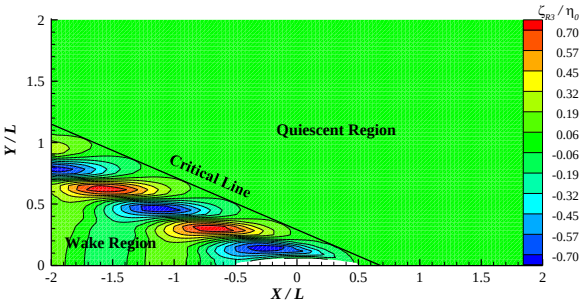

Figure 1 Radiation wave pattern (real part) induced by unit heave motion of a Wigley III hull at $F_n = 0.3$, $\tau = 1.32$.

Figure 1 shows a typical radiated wave pattern induced by unit heave motion of a vessel with forward speed (Yuan et al., 2014). Similar to the steady wave problem, the free surface can also be divided into two regions: wake region confined within a semi-wedge angle θ and quiescent region outside θ. However, for the unsteady ship motion, the range of the wedge is not a constant value. It varies with the parameter τ (Lighthill, 1967; Noblesse, 2001; Noblesse and Hendrix, 1992). For the parameter $\tau > 0.25$, there exists a fan-shape quiescent region in front of the vessel. As τ increases, the range of the fan-shape quiescent region will be expanded. Kashiwagi and Ohkusu (1989, 1991) used the asymptotic wave contour to estimate the side-wall effect. The critical line obtained numerically was presented and compared to the results estimated from asymptotic wave contour. Faltinsen (2006) derived a wave angle to investigate interference between the waves generated by each hull of a multihull vessel.

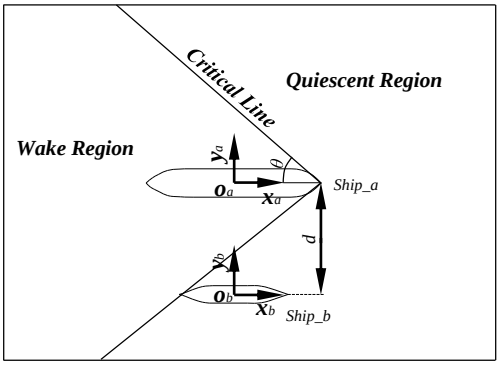

Figure 2 Sketch of ship-to-ship with forward speed problem.

The main objective of the present study is to investigate theoretically and numerically how much in percentage the wave interference is expected. In practice, the ship-to-ship with forward speed problem can well demonstrate the wave interference effects. As shown in Figure 2, when Ship_a is advancing in waves, a critical line can be determined by the asymptotic expressions theoretically. It can be expected if Ship_b is entirely located in the quiescent region of Ship_a, no hydrodynamic interaction is expected. However, the theoretical asymptotic expressions of the far-field wave pattern is based on a single translation and oscillating source point. Due to the 3D effect and local non-radiation waves, the critical line could be different from that obtained theoretically. In order to obtain this real critical line, a massive numerical calculations are required to analyze several combinations of parameters, including oscillation frequency, forward speed and transverse distance between two ships.

Far-field wave patterns and semi-wedge angle

Before numerical calculations, a theoretical estimation should be established based on the asymptotic wave contour. In the present paper, we will use the Havelock form of Green function to investigate the far-field wave patterns generated by a translating and oscillating source in infinite water depth and then establish a rapid estimation of the critical line between the quiescent and wake region. The parametric equations with constant phase can be expressed as

$$\left.\begin{aligned} k_0 x &= \psi_{ij}\frac{2(\kappa_i-\tau)^3-\kappa_i}{(\kappa_i-\tau)^3(\kappa_i+\tau)} \\ k_0|y| &= (-1)^j\psi_{ij}\frac{\sqrt{(\kappa_i-\tau)^4-\kappa_i^2}}{(\kappa_i-\tau)^3(\kappa_i+\tau)} \end{aligned}\right\} \quad (1)$$

where $k_0 = g/u^2$ and (x, y) denotes the position vector of the field point on the free surface. ψ_{ij} is the phase, $\tau = \omega_e u/g$, $\kappa_i = -k_i\cos\theta$ and k_i can be written as

$$k_i = \frac{1}{2\cos^2\theta}\left[1-2\tau\cos\theta+(-1)^i\sqrt{1-4\tau\cos\theta}\right] \quad (2)$$

The quiescent region in Figure 1 and Figure 2 then can be determined by the semi-angle θ, which may be referred as semi-wedge angle hereafter. At $\tau < 0.25$, this semi-angle θ does not exist, since the ring waves could cover the entire computational domain. Therefore, we are only concerned with the case of $\tau > 0.25$ in the present study. The semi-wedge angles of ring waves and inner V waves can be written as (Yuan et al., 2015)

$$\left.\begin{aligned} \theta_r &= \tan^{-1}\left[-\frac{\sqrt{(\nu_5-\tau)^4-\nu_5^2}}{2(\nu_5-\tau)^3-\nu_5}\right] \\ \theta_i &= \tan^{-1}\left[-\frac{\sqrt{(\nu_6-\tau)^4-\nu_6^2}}{2(\nu_6-\tau)^3-\nu_6}\right] \end{aligned}\right\} \quad (3)$$

The values of ν_5 and ν_6 can be found in Noblesse and Hendrix (1992) as

$$\nu_{5,6} = -\frac{\sqrt{2-c+\sqrt{(1-2c)^2+48\tau^2}}}{2} \pm \left(\tau+\sqrt{1+c}/2\right) \quad (4)$$

where

$$c = (16\tau^2-1)^{1/3}\left[\left(1+4\tau\right)^{1/3}+\left(1-4\tau\right)^{1/3}\right]/2 \quad (5)$$

It should also be noted that as $\kappa_i \rightarrow -\tau$, the corresponding semi-wedge angle for the inner fan wave could be expressed as

$$\theta_f = \tan^{-1}\left[(-1)^{j-1}\frac{1}{\sqrt{16\tau^2-1}}\right] \quad (6)$$

The semi-wedge angles defined by Eq. (3) and Eq. (6) are depicted in Figure 3. The semi-wedge angle of the outer V waves is also presented. When it refers to ship-to-ship problem, as shown in Figure 2, two values of τ are of particular interest: $\tau = 0.272$ (the analytical expression is $\sqrt{2/27}$, which can be found in Chen (1998)) and $\tau = 1.62$. At $\tau < 0.272$, the semi-wedge angle $\theta_r > 90°$. In this case, the hydrodynamic interactions between two ships are inevitable and the minimum spacing could not exist. Another critical case is $\tau = 1.62$. As $\tau > 1.62$, the semi-wedge angle $\theta_r < 19.47°$. In this case, the hydrodynamic interactions and the minimum spacing are dominated by the steady waves. The quiescent region could exist outside the Kelvin wedge. In the range of $0.272 < \tau < 1.62$, the quiescent region is determined by θ_r, since θ_i and θ_f are confined within the semi-wedge angle of the ring waves.

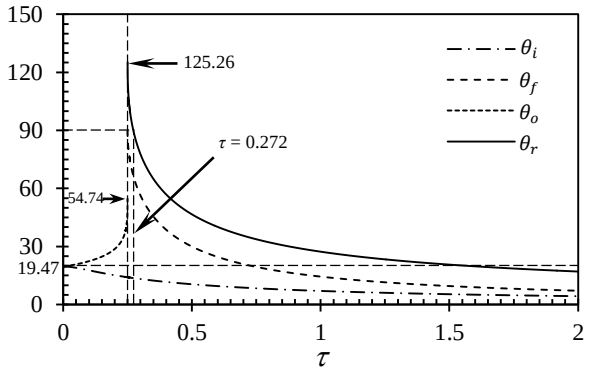

Figure 3 Semi-wedge angles (deg.): θ_r, ring wave system ($\tau > 0.25$); θ_o, outer V wave system ($\tau < 0.25$); θ_i, inner V wave; θ_f, fan wave system ($\tau < 0.25$).

As long as the semi-wedge angle is determined, From Figure 2, we can obtain the minimum spacing between two ships, at which no wave interference is expected. Let's denote the length of the larger and smaller ships as L_a and L_b respectively, the minimum spacing between two ships can be written as

$$d/L_a = \begin{cases} \infty, & (\tau \le 0.272) \\ \dfrac{1}{2}(1+\delta)\dfrac{\sqrt{(\nu_5-\tau)^4-\nu_5^2}}{2(\tau-\nu_5)^3+\nu_5}, & (0.272<\tau<1.62) \\ \dfrac{1}{2}(1+\delta)\tan(19.47^\circ), & (\tau \ge 1.62) \end{cases} \quad (7)$$

where $\delta = L_b/L_a$ is the ratio of the length of Ship_b to Ship_a, and ν_5 is defined in Eq. (4). From Eq. (7), it can be seen that the dimensionless optimum spacing is only determined by δ and τ.

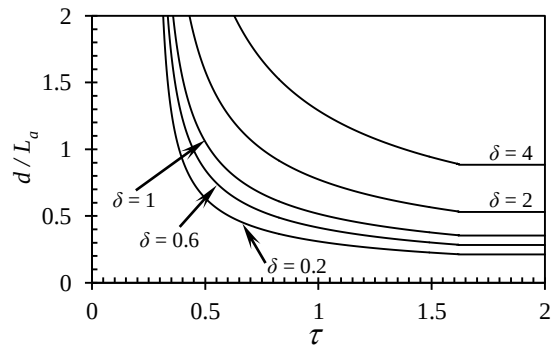

Figure 4 Dimensionless minimum spacing between two advancing ships at δ = 0.2, 0.6, 1, 2, and 4.

Wave interference diagram

In order to validate the above estimation of the semi-wedge angle, we used MHydro, which is based on 3-D Rankine source panel method, to calculate the hydrodynamic properties of two ship advancing in waves. A superposition method is adopted in the

boundary value problem. The total radiation velocity potential is composed of two components: φ^a, which is due to the motion of Ship_a while Ship_b is fixed; φ^b, which is due to the motion of Ship_b while Ship_a is fixed.

The hydrodynamic forces produced by the oscillatory motions of the vessel in the six degrees of freedom can be derived from the radiation potentials as given in the following

$$F_i^{Ra} = \sum_{j=1}^{6}\left[\omega_e^2 A_{ij}^{aa} + i\omega B_{ij}^{aa}\right]\eta_j^a + \sum_{j=1}^{6}\left[\omega_e^2 A_{ij}^{ab} + i\omega B_{ij}^{ab}\right]\eta_j^b ,$$

i=1, 2, …, 6 (8)

$$F_i^{Rb} = \sum_{j=1}^{6}\left[\omega_e^2 A_{ij}^{ba} + i\omega_e B_{ij}^{ba}\right]\eta_j^a + \sum_{j=1}^{6}\left[\omega_e^2 A_{ij}^{bb} + i\omega_e B_{ij}^{bb}\right]\eta_j^b ,$$

i=1, 2, …, 6 (9)

where A and B are the added mass and damping respectively. The superscript 'aa' denotes self-induced radiation force (radiation force on Ship_a due to the motion of Ship_a itself); 'ab' denotes external-induced radiation force (radiation force on Ship_a due to the motion of Ship_b). η_j $(j=1,2,...6)$ is the corresponding motion amplitude. The wave elevation on the free surface then can be obtained from the dynamic free surface boundary condition in the form

$$\zeta_j = \frac{i\omega_e}{g}(\eta_j^a\varphi_j^a + \eta_j^b\varphi_j^b) + \frac{1}{g}\nabla(\varphi_s - u_0 x)\cdot\nabla(\eta_j^a\varphi_j^a + \eta_j^b\varphi_j^b)$$

$$= \zeta_{Rj} + i\zeta_{Ij}\,, \quad j = 0, 1, \ldots, 7 \qquad (10)$$

where ζ_{Rj} is the real part of j-th model, and ζ_{Ij} is the imaginary part.

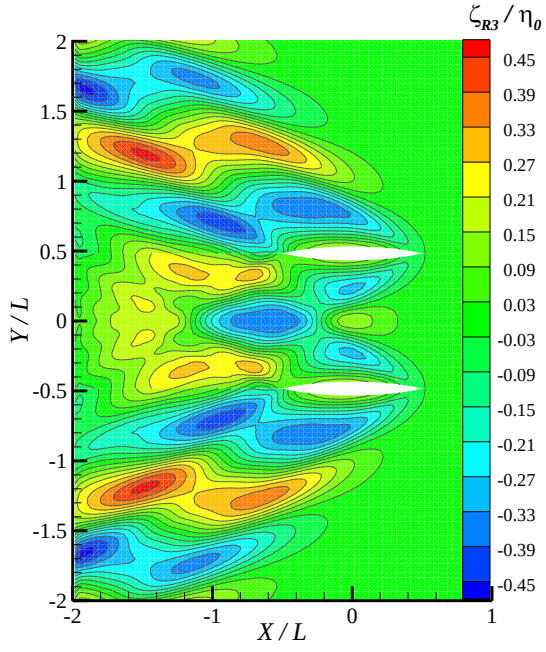

Figure 5 Real part of radiated waves for unit heave motion of two ships advancing in head waves at d / L = 1, τ = 0.521 and F_n = 0.2.

The example models involved in numerical study are two identical Wigley III hulls (δ = 1) with B / L = 0.1.

The factors which determine the hydrodynamic interaction include several combinations of parameters: frequency, forward speed and transverse distance between two ships. Let's firstly examine the wave elevation produced by two travelling ships at d / L = 1. From Figure 4 we can find the assumptive critical τ = 0.521 estimated from the far-field asymptotic wave pattern. Theoretically, no hydrodynamic interactions are expected at τ > 0.521. However, the numerical wave patterns in Figure 5 show the inconsistency with the asymptotic wave contour. In order to observe this inconsistency, we calculated the wave profiles in the portside and starboard of the lower ship in Figure 5. This is presented in Figure 6. According to the asymptotic expression, the wave interference effect diminishes at τ = 0.521 and the wave profiles should be symmetrical. However, the calculated wave profiles violates the theoretical estimation. The identical wave profiles can only be found in the fore part of the ship, while the discrepancies become evident in the stern area.

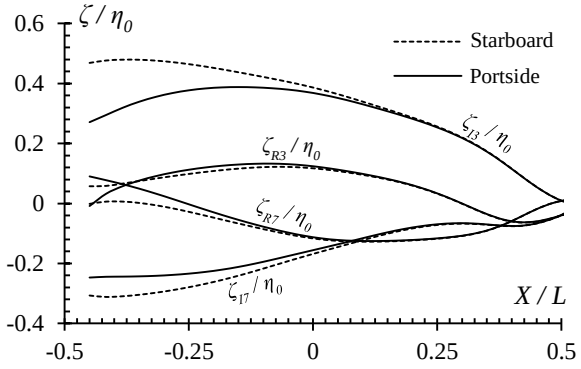

Figure 6 Wave profiles at portside and starboard of the lower ship in Figure 5.

The results in Figure 5 and Figure 6 indicate that the stationary phase method is not able to estimate accurately how the radiated waves propagate to the far-field and how much interactions are expected between two ships travelling in waves. Therefore, an accurate estimation of the critical line is desired, which requires numerous simulations varying Froude number, frequency and transverse distance. A similar approach which was adopted by Kashiwagi and Ohkusu (1991) to investigate the side-wall effects is introduced here to investigate ship-to-ship hydrodynamic interaction effects. In Kashiwagi and Ohkusu's study (1991), the side-wall effects are estimated by the difference between the hydrodynamic coefficients with side-wall and in the open sea. In the present study, we used another parameter to estimate the hydrodynamic interaction effects. That is the external-induced hydrodynamic coefficient A_{ij}^{ab} or B_{ij}^{ab}. These components can directly reflect how much the hydrodynamic interactions are expected, since for the case of single ship, these components do not exist.

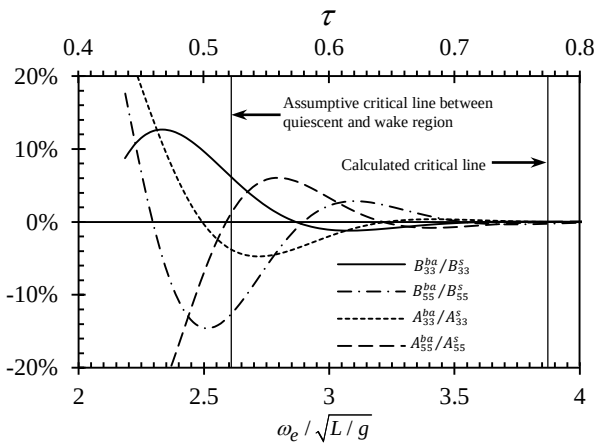

Figure 7 External-induced hydrodynamic coefficients of two identical Wigley hulls at d / L = 1 and F_n = 0.2. The results are presented in percentage and non-dimensionlized by the corresponding values of single vessel in open sea, and the superscript 's' of A_{ij}^{s} or B_{ij}^{s} denotes the single vessel results.

Figure 7 shows the external-induced components of the hydrodynamic coefficients, which is non-dimensionlized by the single ship results. Strictly speaking, there should be 36 inndependent components of each set of external-induced hydrodynamic coefficients if the two ships are not identical. In order to find the region where there is no wave interference, all of these components should be zero. In the numerical calculation, due to the numerical error, these components are impossible to be zero. Therefore, we have to set a permissible error and if the calculation values are bellow this permissible error, no hydrodynamic interaction is expected. In the present study, the permissible error is defined as 0.2%. Coincidently, the calculated results are quite consistent and convergent, even though the different components fluctuate with different amplitudes. Theoretically, no hydrodynamic interactions are expected at $\tau > 0.521$. However, the numerical calculations presented in Figure 7 show a significant hydrodynamic interaction effect at $\tau = 0.521$, and some components even experience an increasing trend at $\tau > 0.521$. The hydrodynamic interaction effects gradually diminish and the external-induced hydrodynamic coefficients are convergent to the permissible error. At $F_n = 0.2$, the curves are convergent to the permissible error at $\tau = 0.773$.

We can determine the critical lines showing the existence of the hydrodynamic interaction effects as a function of Froude number, frequency and transverse distance. Results are shown in Figure 8, where *x*-axis is the $\sqrt{g/L}/\omega_e = F_n/\tau$, *y*-axis is F_n. The ratio of *y* to *x* is parameter τ. In the present numerical calculation, as the two ships are in the same length ($\delta = 1$), for a given value of d / L, the critical parameter τ is unique. Therefore, the dashed lines in Figure 8 are linear and they represent the critical line estimated from the asymptotic far-field wave theory. The solid curves are the calculated critical lines, which approach the dotted lines at high frequency, where the wavelength is relatively small compared to the transverse distance between two ships and the theoretical estimation is valid. As the encounter frequency decreases, the discrepancies become evident and the range of hydrodynamic interaction effects expands. The difference between the dashed lines and solid curves is due to the effect of the near-field non-radiation local waves in the vicinity of the ships.

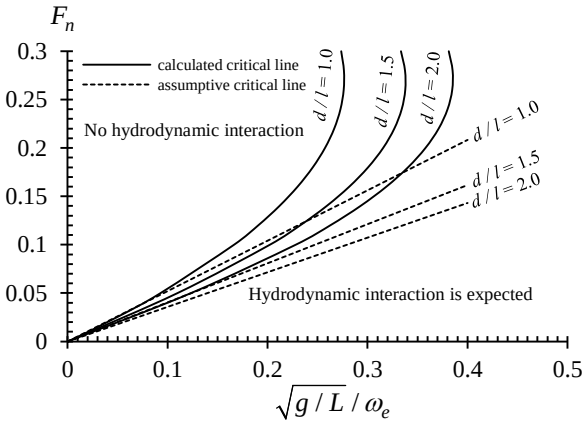

Figure 8 Theoretical and numerical estimation of the critical lines showing whether the ship-to-ship hydrodynamic interaction effects are expected.

The permissible error can be various, for example, 1%. From Figure 7 it can be found the critical parameter τ shifts to a smaller value and the discrepancies between the dashed lines and solid curves become small. However, the selection of the permissible error must be very careful. It should not be very large, for example 5%, otherwise the curves of the hydrodynamic coefficients will be subject to fluctuations before they tend to convergent. On the other hand, the results of different components will be inconsistent and individual diagrams are require.

References

Chen, X.-B., Noblesse, F., 1998. Super Green functions for generic dispersive waves, *IWWWFB13*, Netherlands.

Kashiwagi, M., Ohkusu, M., 1991. A new theory for side-wall interference effects on forward-speed radiation and diffraction forces. *Ship Technology Research* 38 (1), 17-48.

Lighthill, M.J., 1967. On waves generated in dispersive systems by travelling forcing effects, with applications to the dynamics of rotating fluids. *Journal of Fluid Mechanics* 27 (4), 725-752.

Noblesse, F., 2001. Analytical representation of ship waves. *Ship Technology Research* 48, 23-48.

Noblesse, F., Hendrix, D., 1992. On the theory of potential flow about a ship advancing in waves. *Journal of Ship Research* 36 (1), 17-30.

Yuan, Z.-M., Incecik, A., Ji, C.-Y., Zhao, W., Day, A., 2015. Theoretical and numerical estimation of ship-to-ship hydrodynamic interaction effects. Submitted to *Ocean Engineering*.

Yuan, Z.-M., Incecik, A., Jia, L., 2014. A new radiation condition for ships travelling with very low forward speed. *Ocean Engineering* 88, 298-309.